Electrochimica Acta 80 (2012) 302–307

Contents lists available at SciVerse ScienceDirect

Electrochimica Acta

journal homepage: www.elsevier.com/locate/electacta

One step synthesis of Fe_2O_3/nitrogen-doped graphene composite as anode materials for lithium ion batteries

Meng Du, Chaohe Xu, Jing Sun*, Lian Gao

The State Key Lab of High Performance Ceramics and Superfine Microstructure, Shanghai Institute of Ceramics, Chinese Academy of Sciences, 1295 Ding Xi Road, Shanghai 200050, China

ARTICLE INFO

Article history:
Received 24 April 2012
Received in revised form 4 July 2012
Accepted 9 July 2012
Available online 16 July 2012

Keywords:
Iron oxide
Nitrogen-doped graphene
Anode material
Lithium ion batteries

ABSTRACT

Fe_2O_3/nitrogen-doped graphene composite has been synthesized by one-step hydrothermal strategy. Fe_2O_3 particles with size about 100–200 nm uniformly loaded on nitrogen-doped graphene. Fe_2O_3/nitrogen-doped graphene composite shows more excellent cycling performance than those of Fe_2O_3/pristine graphene composite and pure Fe_2O_3, delivering the reversible capacity of 1012 mAh g^{-1} after 100 cycles. Moreover, it shows more superior rate capability, which attains 800 mAh g^{-1} at the current density of 800 mA g^{-1}. The good electrochemical performance can be ascribed to the small particle size of Fe_2O_3, the synergistic effect between Fe_2O_3 particles and nitrogen-doped graphene, and the good electronic conductivity by introducing nitrogen-doped graphene to the composite.

1. Introduction

Graphite is widely commercialized as anode material for lithium ion batteries (LIBs) [1]. Nevertheless, the low theoretical capacity of graphite (372 mAh g^{-1}) limits its applications in high-power electric vehicles [2]. New breakthroughs need be pursued intensively in electrode materials to achieve superior performance. Metal oxides, such as SnO_2, Fe_2O_3, Fe_3O_4, Co_3O_4, Mn_3O_4 and so on, have been developed as new alternative anode materials [3–7]. Among them Fe_2O_3 with high theoretical specific capacity (1005 mAh g^{-1}), low cost and abundant reserve has been regarded as a potential anode material for LIBs. However, the low electrical conductivity and the poor cycling performance due to huge volume changes occurred during lithium insertion/extraction process of Fe_2O_3 particles impede its practical applications [8]. Recent researches indicated that nanostructured electrode materials or carbon coating could help to solve the above two problems. Liu and coworkers synthesized Fe_2O_3 nanorods with diameter of 60–80 nm, which showed a stable specific capacity of 800 mAh g^{-1} [9]. Zhao et al. creatively coated the Fe_2O_3 with single-walled carbon nanohorns, which revealed excellent rate performance and cycle stability [10]. Unfortunately, these strategies just delayed the pulverization of the metal oxide in some degree. In a long time of cycling, the crush of the anode materials still happened. Graphene has been used as matrix to combine with metal oxide for LIBs due to its superior electrical and mechanical properties, large specific surface area (~2600 m^2 g^{-1}) and chemical stability [11,12]. Wang and coworkers successfully obtained Fe_2O_3/graphene composite (Fe_2O_3/G) as the anode materials for LIBs, delivering a high discharge capacity of 660 mAh g^{-1} during up to 100 cycles at the current density of 160 mA g^{-1} and good rate capability [13].

Recently, people utilized nitrogen-doped graphene for lithium anode battery application and received excellent capacity and cyclic performance [14,15]. Nitrogen-doped graphene still kept good mechanical properties as pristine graphene. Additionally, the doped nitrogen atoms can provide extra lone pair electrons and as a result, the electron density of graphene will be augmented which makes the electrical conductivity improved than that of the pristine graphene [16,17]. Moreover, graphene containing nitrogen atoms can induce many surface defects, and as a result the lithium ion can be much easier to get inserted/extracted, leading to the increase of the reversible capacity [14]. Reddy et al. demonstrated that nitrogen-doped graphene prepared by CVD could deliver double capacity compared to that of the pristine graphene [18]. Theoretical studies indicated that the doped nitrogen atoms can be divided into three kinds, pyridinic-like, pyrrolic-like and graphitic-like nitrogen atoms [19–21]. Li et al. demonstrated that the adsorption energy of lithium ions at the pyridinic-like defects was quite large and the energy barrier for lithium penetrating the defects was very low that the capability for lithium storage would be greatly enhanced with such structure [22]. Besides, the nitrogen-doped graphene provides more active and nucleation sites, which facilitate the morphology and particle size control of the hybrids.

Herein, we utilized one-step hydrothermal method to synthesize the Fe_2O_3/nitrogen-doped graphene composite (Fe_2O_3/N-G). TEM revealed that the Fe_2O_3 particles with diameter of 100–200 nm

* Corresponding author. Tel.: +86 12 52414301; fax: +86 21 52413122.
E-mail address: jingsun@mail.sic.ac.cn (J. Sun).

0013-4686/$ – see front matter © 2012 Elsevier Ltd. All rights reserved.
http://dx.doi.org/10.1016/j.electacta.2012.07.029

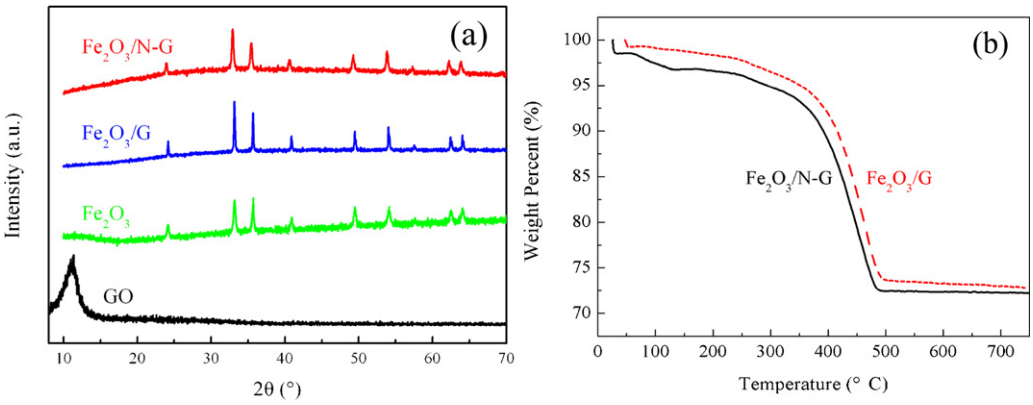

Fig. 1. (a) XRD patterns of GO, pure Fe_2O_3, Fe_2O_3/G and Fe_2O_3/N-G. (b) TG analyses of Fe_2O_3/G and Fe_2O_3/N-G measured from 25 to 750 °C at a heating rate of 10 °C min^{-1} in air.

uniformly decorated on the nitrogen-doped graphene. The XPS results demonstrated that the nitrogen atoms successfully doped in the Fe_2O_3/N-G after hydrothermal procedure. With the synergistic effect of Fe_2O_3 and nitrogen-doped graphene, the composite showed a high reversible specific capacity, superior rate capability and outstanding cycling stability as anode materials for LIBs.

2. Experimental

2.1. Preparation of samples

Graphene oxide (GO) was prepared by the modified Hummers method [3,23]. In a typical synthesis, 1.6 g of $Fe(NH_4)_2(SO_4)_2{\cdot}6H_2O$ was added into 100 mL GO solution (1 mg mL^{-1}) followed by stirring for 10 min. Then, the solution was transferred into a Teflon-lined autoclave and heated at 180 °C for 6 h. Finally, the resulting composite was washed with deionized water for several times, and then dried in a vacuum oven at 60 °C for 10 h. The Fe_2O_3/G was prepared for comparison in the same procedure while replacing $Fe(NH_4)_2(SO_4)_2{\cdot}6H_2O$ with $FeSO_4{\cdot}7H_2O$. Pure Fe_2O_3 was also prepared with $FeSO_4{\cdot}7H_2O$ and NaOH.

2.2. Materials characterization

The phase identification of the Fe_2O_3/N-G, Fe_2O_3/G and pure Fe_2O_3 was performed on the powder X-ray diffraction (XRD) pattern with Cu Kα irradiation. The ac impedance spectra were tested on electrochemical workstation (PARSTAT 2273). Four probe measurements was carried out on the tester (Accent 5500). Morphological observation was carried out using a transmission electron microscope (TEM, JEM-2100F at 200 kV) and field-emission scanning electron microscope (SEM, JEOL-6300F at 1 kV). Thermogravimetry (TG) analysis was performed by using a STA409/PC simultaneous thermal analyzer (Netzsch, Germany) in air with a temperature range of 25–750 °C. The XPS data were taken on a VG SCIENTIFIC 310F in the range of 0–1350 eV.

2.3. Electrochemical measurements

The electrochemical experiments of the Fe_2O_3/N-G, Fe_2O_3/G and pure Fe_2O_3 were performed using R 2025 type coin cells. The test electrodes were prepared by mixing the active materials, acetylene black, and polyvinylidene fluoride (PVDF) binder in weight ratio of 80:10:10, and later dispersed in N-methyl-2-pyrrolidone (NMP). The electrolyte used was 1 M $LiPF_6$ in a 50:50 weight ratio ethylene carbonate (EC):dimethyl carbonate (DMC) solvent (Zhangjiagang Guotai-Huarong New Chemical Materials Co., Ltd.). The cells were assembled in an argon-filled glovebox (MBRAUN) and galvanostatically discharged and charged using a CT 2001 battery tester in room temperature.

3. Results and discussion

The XRD patterns of the GO, Fe_2O_3, Fe_2O_3/G and Fe_2O_3/N-G are shown in Fig. 1a. Due to the presence of oxygenated functional groups, the *d*-spacing of GO calculated from the (0 0 1) peak is approximately 0.85 nm ($2\theta = 11^\circ$) similar to the reported result [24]. The sharp peaks of Fe_2O_3, Fe_2O_3/G and Fe_2O_3/N-G indicate that the Fe_2O_3 particles are well crystallized (JCPDS 33-0664). GO has been converted to graphene in the hydrothermal process. The peak of graphene at ~25° almost overlaps with the main peak of Fe_2O_3 (0 1 2). Fig. 1b exhibits the TG analysis of the Fe_2O_3/G and Fe_2O_3/N-G. The weight loss between 25–120 °C and 220–480 °C can be ascribed to the loss of absorbed water and the pyrolysis of graphene, respectively. The mass loading of graphene is as the same as ~25 wt% in Fe_2O_3/G and Fe_2O_3/N-G composites.

Fig. 2 shows the TEM images of the as prepared Fe_2O_3 (a), composites of Fe_2O_3/G (b) and Fe_2O_3/N-G (c). Pure Fe_2O_3 crystal has particle size about 1 μm. The presence of GO in hydrothermal process decreased the particle size of Fe_2O_3 obviously. As clearly shown in Fig. 2b, the particle size of Fe_2O_3 in Fe_2O_3/G is much smaller than that in Fig. 2a, although it has a wide size distribution of 100–500 nm (Fig. 2d). Nitrogen-doped graphene with more defects than pristine graphene provides more nucleating sites for Fe_2O_3 and as a result Fe_2O_3 particles loaded on nitrogen-doped graphene have uniform size of 100–200 nm (Fig. 2d). The homogenous distribution of finer Fe_2O_3 particles on nitrogen-doped graphene will play an important role in electrochemical process.

The XPS and Raman experiments are conducted to analyze the chemical binding state of the samples. Fig. 3a shows the XPS spectra of GO, Fe_2O_3/G and Fe_2O_3/N-G. The peaks appeared at 285.0, 399.9 and 531.9 eV can be assigned to C 1s, N 1s and O 1s, respectively. There is no obvious N 1s peak in the XPS spectrum of GO or Fe_2O_3/G. The N 1s peak of Fe_2O_3/N-G can prove that the nitrogen atoms have doped in graphene after the hydrothermal process. When the temperature gets to 180 °C, the NH_4^+ coming from $Fe(NH_4)_2(SO_4)_2$ will attack the oxygen-containing functional groups and combines with graphene by dehydration, nitrogen atoms stayed on carbon loops. In Fig. 3b it shows clearly that the peak represents C sp^3 atoms of GO almost disappeared after the hydrothermal process. It demonstrates that hydrothermal reaction can help graphene to get rid of the oxygenated functional groups connected with the C sp^3 atoms [25]. The N 1s XPS spectrum of Fe_2O_3/N-G can be split to three component peaks centered at about 401.2 eV (graphitic-like nitrogen), 399.8 eV (pyrrolic-like nitrogen) and 398.5 eV

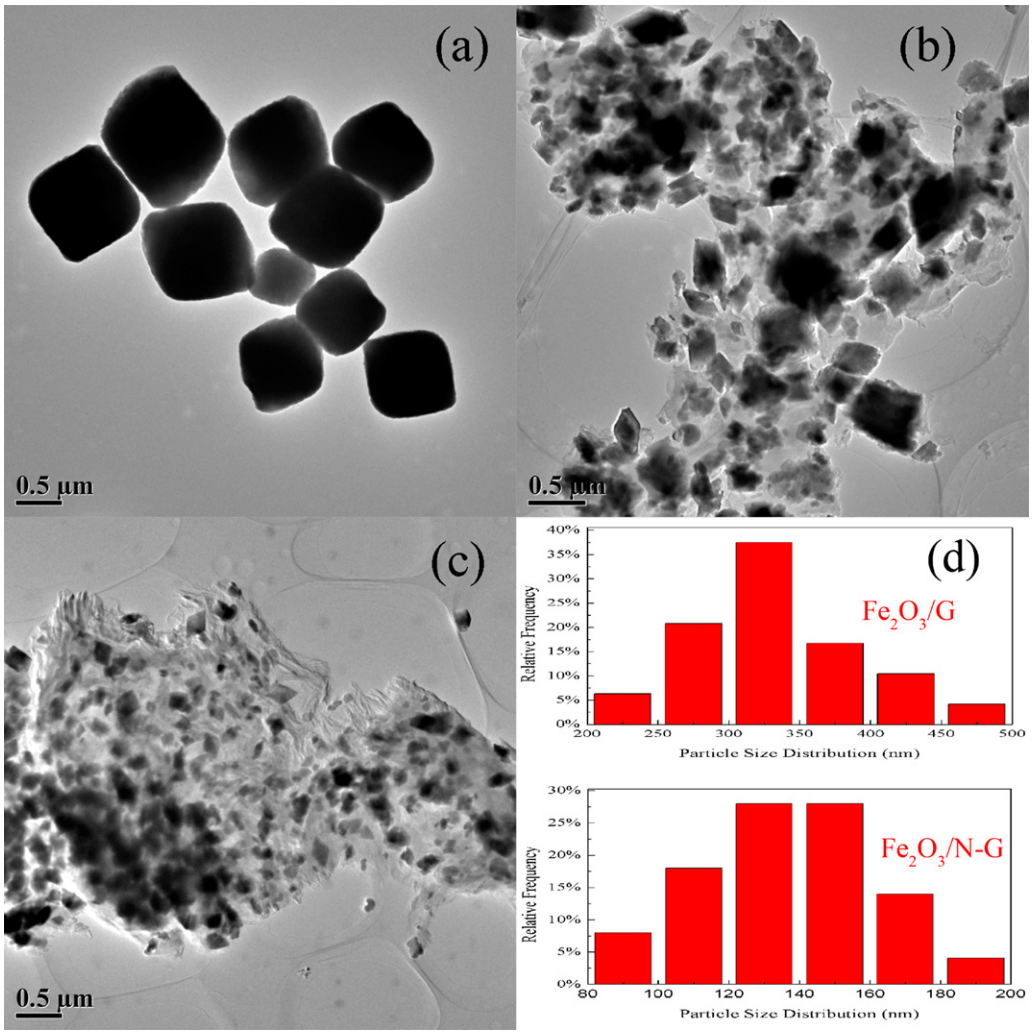

Fig. 2. TEM images of pure Fe_2O_3 (a), Fe_2O_3/G (b), and Fe_2O_3/N-G (c), (d) histograms of Fe_2O_3 particle size distribution in composites of Fe_2O_3/G and Fe_2O_3/N-G.

(pyridinic-like nitrogen), respectively [19,26]. There is no obvious peak of GO and Fe_2O_3/G around 399.9 eV as shown in Fig. 3c. C, O and N contents of GO, Fe_2O_3/G and Fe_2O_3/N-G are presented in Table 1. The atomic ratio of N/C is considered to describe the nitrogen content in graphene [27]. It sharply increases from 0.0047 of GO, 0.0078 of Fe_2O_3/G to 0.0325 of Fe_2O_3/N-G, which indicates that the nitrogen atoms originated from NH_4^+ took the place of the carbon atoms on graphene nanosheets through hydrothermal reaction. The Raman spectra in Fig. 3d can also prove the nitrogen-doping phenomenon. The G peak represents the intrinsic peak of C sp^2 atoms, while the D peak is caused by the defects associated with vacancies and grain boundaries [28]. From GO to Fe_2O_3/G the intensity ratio of the D over the G band (I_D/I_G) slightly decreases, which is an indication of the disappearance of C sp^3 atoms after hydrothermal. Compared with the Fe_2O_3/G, the I_D/I_G of the Fe_2O_3/N-G obviously increased after the same hydrothermal process. Nitrogen doping in the graphene led to the increase of D band.

Table 1
Element content of C, O and N estimated from XPS data and the N/C atom ratios.

Samples	C (wt%)	O (wt%)	N (wt%)	N/C (at./at.)
GO	64.4	34.6	0.3	0.0047
Fe_2O_3/G	64.0	28.2	0.5	0.0078
Fe_2O_3/N-G	67.7	27.3	2.2	0.0325

Fig. 4 shows the Nyquist plots of the cells with pure Fe_2O_3, Fe_2O_3/G and Fe_2O_3/N-G anodes at a discharged potential of 0.1 V. It is usually considered that the charge-transfer resistance can be signified by the semicircle in the medium-frequency region [29]. Although the materials are combined with carbon black (as conductive additive), it is obviously that the existence of graphene improves the conductivity of pure Fe_2O_3 a lot. As can be seen from the ac impedance spectra, Fe_2O_3/N-G performs much higher conductivity than that of Fe_2O_3/G owning to the super conductivity of the nitrogen-doped graphene compared with the pristine graphene. Four probe method was applied to measure the conductivity as well, and the conductivities of Fe_2O_3, Fe_2O_3/G and Fe_2O_3/N-G are 0.00298 S m^{-1}, 10.3 S m^{-1} and 19.2 S m^{-1}, respectively. By hybridizing with graphene, the conductivity of Fe_2O_3 increased three orders of magnitude, and the conductivity of Fe_2O_3/N-G is about one time higher than that of Fe_2O_3/G [17].

After 100 times of cycling at the current density of 100 mA g^{-1}, the TEM image of Fe_2O_3/N-G material was shown in Fig. 5a. The structures of Fe_2O_3 particles still remain the same. The particle size of Fe_2O_3 increased slightly to about 120–220 nm (Fig. 5b). The small particle size and excellent conductivity of Fe_2O_3/N-G kept it from pulverization.

The cyclic voltammetry (CV) curves of Fe_2O_3/N-G at 1st, 2nd, and 5th cycles in the voltage window of 3–0 V at scan rate of 0.5 mV s^{-1} are shown in Fig. 6a. In the 1st cycle, the cathodic peak around 0.7 V corresponds to the conversion reaction of

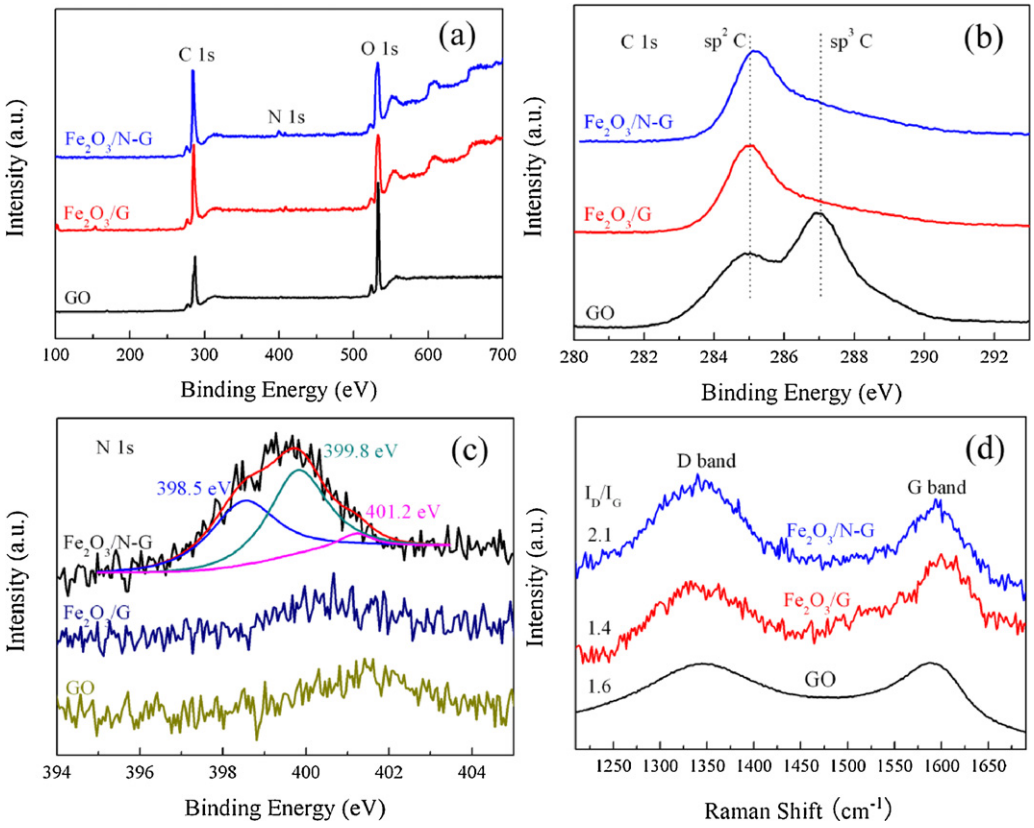

Fig. 3. (a) XPS spectra, (b) C 1s XPS spectra, (c) N 1s XPS spectra and (d) Raman spectra of GO, Fe_2O_3/G and Fe_2O_3/N-G. The N 1s peak of Fe_2O_3/N-G can be split to three Lorentzian peaks at 401.2, 399.8, and 398.5 eV, which represent the graphitic-like nitrogen, pyrrolic-like nitrogen and pyridinic-like nitrogen species.

$Fe_2O_3 + 6Li^+ + 6e^- \rightarrow 2Fe^0 + 3Li_2O$ [30]. Beyond the voltage of 0.7 V, there is a sloping curve down to the cutoff voltage of 0.01 V. The exceeded capacity may due to two reasons. One is the decomposing of the solid electrolyte interface (SEI) film gradually. The other reason is the reaction between lithium and the oxygen groups of the graphene, which is called the interface lithium storage. The anodic peak presented around 1.7 V represents the oxydic reaction from Fe^0 to Fe^{3+}. In the 2nd and 5th cycles, the intensity of the cathodic and anodic peaks decrease compared with the 1st cycle, which indicates that the irreversible reactions occur in the 1st cycle. The lithium storage properties of Fe_2O_3, Fe_2O_3/G and Fe_2O_3/N-G with voltage window between 3.0 V and 0.01 V (vs. Li^+/Li) are shown in Fig. 6b–d. Fig. 6b reveals the charge/discharge curves of the Fe_2O_3/N-G at the current density of 100 mA g^{-1}. The initial discharge and charge capacities of the composite are 1442 and 947 mAh g^{-1}, respectively. The coulombic efficiency is ~66%. The voltage plateau at ~0.85 V of the first discharge curve can be attributed to the forming of SEI layers on the graphene surface, which usually happened as with the carbon-based electrodes in the 1st cycle [31,32]. Fig. 6c shows the rate capability of Fe_2O_3, Fe_2O_3/G and Fe_2O_3/N-G at different current densities, the specific capacity of Fe_2O_3/N-G exceeds those of the other two materials. At the current density of 800 mA g^{-1}, the discharge/charge capacities of Fe_2O_3/N-G are as high as ~800 mAh g^{-1}, which are much higher than that of Fe_2O_3/G (~220 mAh g^{-1}) and Fe_2O_3 (~40 mAh g^{-1}). As we know, the conductivity of anode materials plays an important role in electron transmission, especially in high rate current density. Fig. 6d shows the cycling performance of Fe_2O_3/N-G at 100 mA g^{-1}. After 100 cycles, Fe_2O_3/N-G can deliver a reversible capacity of 1012 mAh g^{-1}, the coulombic efficiency of Fe_2O_3/N-G remains above 97%. In order to investigate the electrochemical performance of nitrogen-doped graphene composite deeply, cycle performance of the electrodes of pure Fe_2O_3, Fe_2O_3/G are also investigated for comparison in our experiments (Fig. 6d). In the charge process, lithium ions diffuse into the anode materials and the higher conductivity facilitate faster ions diffusion, leading to higher specific capacity. When lithium ions insert into the anode materials, the volume of them will expand in some degree. The smaller size of Fe_2O_3 particles will tolerate the volume expanding and achieve higher cycling stability. The cycle performance indicates that Fe_2O_3 and the Fe_2O_3/G composite can only deliver a reversible capacity of ~200 mAh g^{-1} and ~430 mAh g^{-1} after 100 cycles, respectively. When nitrogen-doped graphene was introduced to the composite, the reversible capacity is enhanced

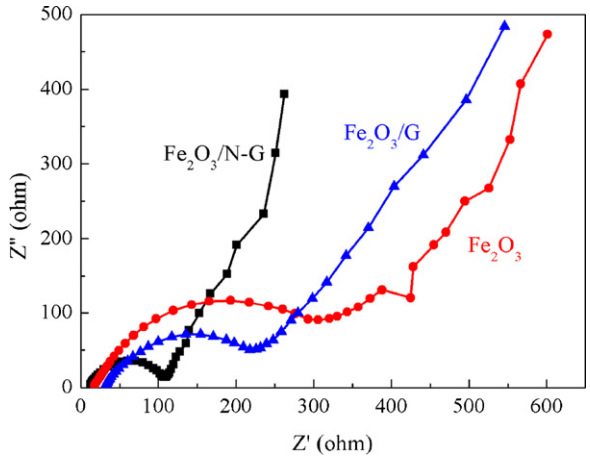

Fig. 4. Nyquist plots of pure Fe_2O_3, Fe_2O_3/G and Fe_2O_3/N-G anodes at a discharged potential of 0.1 V (vs. Li/Li^+) from 100 kHz to10 mHz.

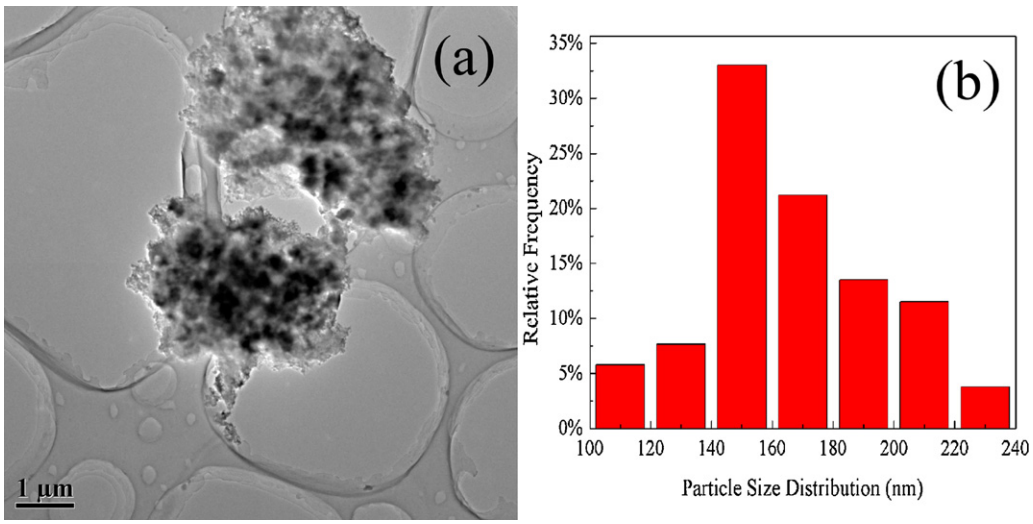

Fig. 5. (a) TEM image and (b) histogram of Fe_2O_3 particle size distribution in composite of Fe_2O_3/N-G after 100 times cycling at the current density of 100 mA g^{-1}.

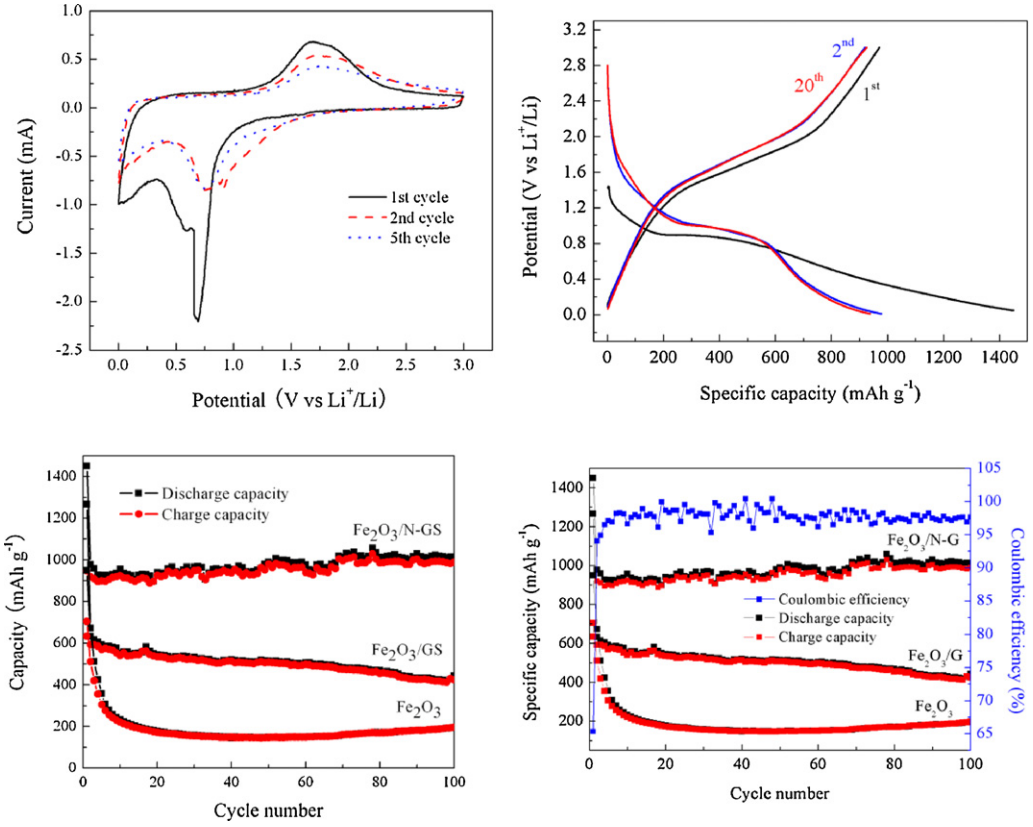

Fig. 6. (a) Cyclic voltammograms of Fe_2O_3/N-G for the 1st, 2nd, and 5th cycles at a scan rate of 0.5 mV s^{-1} with a voltage window from 3 to 0 V. (b) Lithium insertion/extraction properties of Fe_2O_3/N-G. (c) The charge/discharge performance of pure Fe_2O_3, Fe_2O_3/G and Fe_2O_3/N-G at various current rates. (d) The coulombic efficiency of Fe_2O_3/N-G and the cycling performances of pure Fe_2O_3, Fe_2O_3/G and Fe_2O_3/N-G at the current density of 100 mA g^{-1}.

markedly, which can mainly be ascribed to two reasons. Firstly, more nucleation sites of the nitrogen-doped graphene can make the Fe_2O_3 particles smaller and more uniform, which can shorten the distance of lithium ion diffusion. Secondly, the high lithium storage property of the nitrogen-doped graphene helped to improve the synergistic effect between Fe_2O_3 particles and nitrogen-doped graphene.

4. Conclusions

In summary, Fe_2O_3/N-G has been synthesized as anode materials for LIBs by one-step hydrothermal procedure. The presence of nitrogen-doped graphene helps Fe_2O_3 particles formed with smaller size and homogenous distribution. The hybrid composite with good electrical conductivity shows a high reversible specific

capacity, superior rate capability and outstanding cycling stability as anode materials for LIBs. After 100 cycles the reversible capacity of Fe_2O_3/N-G anode still remains 1012 mAh g^{-1}, which is much higher than that of Fe_2O_3 and Fe_2O_3/G. At the current density of 800 mA g^{-1}, its reversible capacity reaches 800 mAh g^{-1}.

Acknowledgements

This work is supported by the National Basic Research Program of China (2012CB932303) and the National Natural Science Foundation of China (Grant No. 51072215 and 51172261).

Appendix A. Supplementary data

Supplementary data associated with this article can be found, in the online version, at http://dx.doi.org/10.1016/j.electacta.2012.07.029

References

[1] H. Buqa, D. Goers, M. Holzapfel, M.E. Spahr, P. Novak, Journal of Electrochemical Society 152 (2005) A474.
[2] J.M. Tarascon, M. Armand, Nature 414 (2001) 359.
[3] X. Zhu, Y. Zhu, S. Murali, M.D. Stoller, R.S. Ruoff, ACS Nano 5 (2011) 3333.
[4] B. Li, H. Cao, J. Shao, M. Qu, J.H. Warner, Journal of Materials Chemistry 21 (2011) 5069.
[5] B. Li, H. Cao, J. Shao, G. Li, M. Qu, G. Yin, Inorganic Chemistry 50 (2011) 1628.
[6] H. Wang, L.-F. Cui, Y. Yang, H.S. Casalongue, J.T. Robinson, Y. Liang, Y. Cui, H. Dai, Journal of the American Chemical Society 132 (2010) 13978.
[7] C.-H. Yim, E.A. Baranova, F.M. Courtel, Y. Abu-Lebdeh, I.J. Davidson, Journal of Power Sources 196 (2011) 9731.
[8] X.J. Zhu, Z.P. Guo, P. Zhang, G.D. Du, R. Zeng, Z.X. Chen, S.A. Li, H.K. Liu, Journal of Materials Chemistry 19 (2009) 8360.
[9] H. Liu, G.X. Wang, J. Park, J.Z. Wang, H.K. Liu, C. Zhang, Electrochimica Acta 54 (2009) 1733.
[10] Y. Zhao, J. Li, Y. Ding, L. Guan, Chemical Communications 47 (2011) 7416.
[11] J.S. Bunch, A.M.v.d. Zande, S.S. Verbridge, L.W. Frank, D.M. Tanenbaum, J.M. Parpia, H.G. Craighead, P.L. McEuen, Science 315 (2007) 490.
[12] E.J. Yoo, J. Kim, E. Hosono, H.S. Zhou, T. Kudo, I. Honma, Nano Letters 8 (2008) 2277.
[13] G. Wang, T. Liu, Y.J. Luo, Y. Zhao, Z.Y. Ren, J.B. Bai, H. Wang, Journal of Alloys and Compounds 509 (2011) L216.
[14] H. Wang, C. Zhang, Z. Liu, L. Wang, P. Han, H. Xu, K. Zhang, S. Dong, J. Yao, G. Cui, Journal of Materials Chemistry 21 (2011) 5430.
[15] Li-Feng Cui, Riccardo Ruffo, Candace K. Chan, Hailin Peng, Y. Cui, Nano Letters 9 (2009) 491.
[16] Y. Qiu, X. Zhang, S. Yang, Physical Chemistry Chemical Physics 13 (2011) 12554.
[17] Z.-S. Wu, W. Ren, L. Xu, F. Li, H.-M. Cheng, ACS Nano 5 (2011) 5463.
[18] A.L.M. Reddy, A. Srivastava, S.R. Gowda, H. Gullapalli, M. Dubey, P.M. Ajayan, ACS Nano 4 (2010) 6337.
[19] D. Deng, X. Pan, L. Yu, Y. Cui, Y. Jiang, J. Qi, W.-X. Li, Q. Fu, X. Ma, Q. Xue, G. Sun, X. Bao, Chemistry of Materials 23 (2011) 1188.
[20] D. Wei, Y. Liu, Y. Wang, H. Zhang, L. Huang, G. Yu, Nano Letters 9 (2009) 1752.
[21] D. Long, W. Li, L. Ling, J. Miyawaki, I. Mochida, S.H. Yoon, Langmuir 26 (2010) 16096.
[22] Y.F. Li, Z. Zhou, L.B. Wang, Journal of Chemical Physics 129 (2008) 104703.
[23] C.H. Xu, J. Sun, L. Gao, Journal of Materials Chemistry 21 (2011) 11253.
[24] W. Shi, J. Zhu, D.H. Sim, Y.Y. Tay, Z. Lu, X. Zhang, Y. Sharma, M. Srinivasan, H. Zhang, H.H. Hng, Q. Yan, Journal of Materials Chemistry 21 (2011) 3422.
[25] Y. Zhou, Q. Bao, L.A.L. Tang, Y. Zhong, K.P. Loh, Chemistry of Materials 21 (2009) 2950.
[26] M. Pflughoefft, H. Weller, Journal of Physical Chemistry B 106 (2002) 10530.
[27] K.P. Gong, F. Du, Z.H. Xia, M. Durstock, L.M. Dai, Science 323 (2009) 760.
[28] A.C. Ferrari, J.C. Meyer, V. Scardaci, C. Casiraghi, M. Lazzeri, F. Mauri, S. Piscanec, D. Jiang, K.S. Novoselov, S. Roth, A.K. Geim, Physical Review Letters 97 (2006) 187401.
[29] H. Xiang, K. Zhang, G. Ji, J.Y. Lee, C. Zou, X. Chen, J. Wu, Carbon 49 (2011) 1787.
[30] C. Combelles, M.B. Yahia, L. Pedesseau, M.-L. Doublet, Journal of Physical Chemistry C 114 (2010) 9518.
[31] H. Liu, G. Wang, D. Wexler, J. Wang, Electrochemistry Communications 10 (2008) 165.
[32] M. Zhang, D. Lei, X. Yin, L. Chen, Q. Li, Y. Wang, T. Wang, Journal of Materials Chemistry 20 (2010) 5538.